Evaluation of Polarimetric SAR Despeckling Methods for Crop Classification from RCM Compact Polarimetry Data

Ramin Farhadiani[1] and Saeid Homayouni[1]

[1]Centre Eau Terre Environnement, Institut National de la Recherche Scientifique, Québec, QC, Canada - (ramin.farhadiani, saeid.homayouni)@inrs.ca

Keywords: RCM, Compact Polarimetry, Speckle Reduction, Crop Classification, Random Forest.

Abstract

The presence of speckle in RADARSAT Constellation Mission (RCM) Compact Polarimetry (CP) Synthetic Aperture Radar (SAR) images can impair the performance of information extraction applications such as classification. Therefore, a critical preprocessing step known as despeckling is necessary to mitigate this granular, noise-like phenomenon in these images. This paper compared several PolSAR speckle reduction methods, including Box Car, IDAN, Lee Refined, Lee Sigma, Improved Lee Sigma, and Lopez filters. A CP SAR dataset collected over agricultural land in southern Quebec, QC, Canada, was utilized for the study. The assessment of despeckling was based on various no-reference quantitative indicators. Each despeckling method was evaluated for its effectiveness in reducing speckle in homogeneous areas, preserving details, and avoiding radiometric distortion. Additionally, the impact of despeckling on the classification of this agricultural land was assessed using the Random Forest classifier. The Stokes parameters, m-chi decomposition, and intensity images were utilized for this purpose. Experimental results indicated that the Box Car method excelled in speckle suppression at the expense of edge over-smoothing. Furthermore, the Lee Sigma and Improved Lee Sigma methods were the most effective in speckle reduction from homogeneous areas while preserving edges and preventing radiometric distortion. Moreover, the classification results demonstrated that appropriate despeckling could significantly enhance classification accuracy.

1. Introduction

The Canadian RADARSAT Constellation Mission (RCM), launched on June 12, 2019, represents a significant advancement in Synthetic Aperture Radar (SAR) technology, particularly with its ability to obtain Compact Polarimetry (CP) data. However, despite their advantages, such as day/night and all-weather imaging, the CP SAR systems are affected by a granular noise-like phenomenon known as speckle, which is inherent in all coherent imaging systems. The speckle reduces the radiometric quality of SAR images, making their analysis and interpretation more complex (Lee, 1981, Lee et al., 1999). The data's quality and reliability significantly influence the final product's accuracy (Farhadiani et al., 2019b). Therefore, a crucial preprocessing step known as despeckling is required to remove speckle from the SAR images.

Speckle reduction in single polarization (Farhadiani et al., 2022, Wang and Guo, 2023) and full polarimetric (Mullissa et al., 2022, Luo et al., 2023) SAR images have been an extensive research topic in the Remote Sensing community and various despeckling techniques for (Pol)SAR images have been proposed to achieve a balanced trade-off between reducing speckle and preserving details. However, due to the unique nature of the RCM CP data, no speckle reduction method has been specifically developed for this type of SAR data. Surprisingly, only one research was conducted on the despeckling of the simulated CP SAR data (Foucher et al., 2012). Using the simulated CP SAR data could have limitations since it might not accurately reflect real-world properties. Hence, despeckling algorithms tested on the simulated CP data might not perform well when used with the actual CP data. This discrepancy highlights the necessity for additional empirical research using real CP data to verify the robustness and reliability of the despeckling methods. Thus, this study would significantly enhance the understanding in this regard by offering a precise evaluation of the strengths and weaknesses of despeckling methods that were not initially proposed for the CP SAR data. Therefore, the primary goal of this paper is to investigate not only the effectiveness of polarimetric despeckling filters in suppressing speckle from real CP data but also to examine the impact of speckle reduction in crop classification, a critical Remote Sensing application.

2. Methodology

2.1 CP SAR Data

The scattering information in the CP mode is represented using a C2 covariance matrix (Dey et al., 2021), expressed as follows:

$$\mathrm{C2} = \begin{bmatrix} \mathrm{C11} & \mathrm{C12} \\ \mathrm{C21} & \mathrm{C22} \end{bmatrix} = \begin{bmatrix} \langle |E_{RH}|^2 \rangle & \langle E_{RH} E_{RV}^* \rangle \\ \langle E_{RV} E_{RH}^* \rangle & \langle |E_{RV}|^2 \rangle \end{bmatrix} \quad (1)$$

where R indicates that the signal is transmitted in right-hand circular form, while H and V show the received backscattered signal in horizontal and vertical polarizations, respectively.

A set of distinct features has been developed that are crucial for advanced CP data interpretation. In this paper, Stokes parameters and m-chi decomposition (Raney et al., 2012), along with intensity images, i.e., diagonal elements of the C2 matrix, were used for the analysis. Table (1) presents the formula for computing the Stokes parameters and m-chi decomposition.

Moving forward, the study area, shown in Figure 1, is an agricultural land in southern Quebec, QC, Canada. The CP data from all three satellites, i.e., RCM1, RCM2, and RCM3, were

Table 1. CP features used for the classification.

Feature Name	Formula
Intensity	$C11 = \|E_{RH}\|^2, C22 = \|E_{RV}\|^2$
Stokes Parameters	$S_0 = \|E_{RH}\|^2 + \|E_{RV}\|^2$ $S_1 = \|E_{RH}\|^2 - \|E_{RV}\|^2$ $S_2 = 2\mathrm{Re}(E_{RH}E_{RV}^*)$ $S_3 = -2\mathrm{Im}(E_{RH}E_{RV}^*)$
m-chi Decomposition	$m_{\chi_{\mathrm{Blue}}} = \sqrt{S_0 m \frac{(1-\sin 2\chi)}{2}}$ $m_{\chi_{\mathrm{Red}}} = \sqrt{S_0 m \frac{(1+\sin 2\chi)}{2}}$ $m_{\delta_{\mathrm{Green}}} = \sqrt{S_0(1-m)}$
$\sin 2\chi = -\frac{S_3}{mS_0}, \quad m = \frac{\sqrt{S_1^2+S_2^2+S_3^2}}{S_0}$	

obtained during an ascending orbit pass and utilized a high-resolution Stripmap beam mode, offering detailed imagery over a swath width of 30 kilometers. The acquisitions occurred sequentially across the summer of 2021, with RCM1 collecting data on July 1, RCM2 on July 30, and RCM3 on August 27, at a resolution of 5 meters.

Figure 2 demonstrates the workflow adopted in the paper. Initially, all three raw CP data were calibrated into Sigma Naught. Subsequently, the C2 matrix was generated. Following this, various polarimetric despeckling filters in SNAP (European Space Agency, 2024) (i.e., Box Car, IDAN (Vasile et al., 2006), Lee Refined (Lee et al., 1999), and Improved Lee Sigma (Lee et al., 2009)) and PolSARpro (Pottier et al., 2018) (i.e., Lee Sigma (Lee, 1983) and Lopez (Lopez-Martinez and Fabregas, 2008)) with different parameters were applied to the C2 matrix. It should be noted that the RCM3 data is chosen as the CP image for the despeckling evaluation and analysis because this image has stronger and distinguishable edges and details compared to the images obtained using RCM1 and RCM2 satellites. Figure 3 demonstrates the RCM3 image before terrain correction and coregistration, and the corresponding region of interest used for despeckling performance evaluation. Following the despeckling of the C2 matrix, terrain correction and coregistration were performed, and a suitable area was selected for further analysis. The Stokes parameters and the m-chi decomposition were also extracted as CP features and incorporated into the classification process along with intensity CP images across the three CP dates. The Random Forest classifier was employed for this purpose.

2.2 PolSAR Despeckling Methods

2.2.1 Box Car: The boxcar filter applies incoherent averaging of the covariance/coherency matrix across pixels within a neighborhood defined by a sliding window. This filter offers optimal performance in homogeneous areas. However, it tends to blur sharp edges and overfilter point scatterers, transforming them into spread targets.

2.2.2 IDAN: This filter builds upon the concepts from the Lee Refined method. Unlike the traditional filtering methods involve selecting pixels from homogeneous areas within a fixed-size sliding window, which often does not provide enough pixels to reduce estimation variance sufficiently, the IDAN filter avoids restricting pixel selection to a fixed window size. Instead, it employs the region growing technique along with criteria from the Lee sigma filter. For each pixel, an adaptive neighborhood is defined through region growing, and the pixel is then processed using the MMSE (Minimum Mean Square Error) filter, which utilizes all selected pixels.

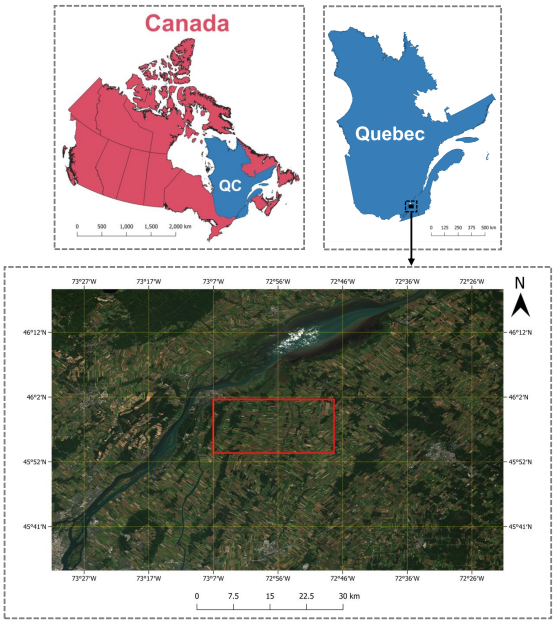

Figure 1. Study area location: southern Quebec, QC, Canada.

2.2.3 Lee Refined: To address the issue of insufficient speckle noise reduction near strong edges, the Lee Refined filter employs non-square windows that align with edge directions. This filter operates within an N×N sliding window. Among eight possible edge-aligned windows, one is chosen to filter the center pixel. Only the pixels in non-edge areas within the selected edge-aligned window are utilized for the filtering computation.

2.2.4 Lee Sigma: The Lee Sigma filter assumes a Gaussian noise distribution and filters the center pixel in a sliding window by averaging the pixels within the two-sigma range. A significant limitation of this algorithm is the consistent underestimation of the mean of pixels within this range. This underestimation arises because the noise distributions are not symmetric, yet symmetric thresholds are applied in selecting the pixels for averaging.

2.2.5 Improved Lee Sigma: The Improved Lee Sigma filter enhances the original Lee Sigma filter. To address the bias problem, it redefined the sigma range according to the probability density functions of the speckle. Target signature preservation was utilized to prevent the filtering of point targets. The MMSE estimator was also employed for adaptive speckle reduction.

2.2.6 Lopez: This filter leverages the multiplicative-additive speckle noise model tailored for multi-dimensional SAR data. In this approach, the entries of the sample Covariance matrix are processed according to this speckle noise model, with modifications based on the complex correlation coefficient. This method allows for differentiated processing of the covariance matrix elements, enhancing speckle noise reduction and improving the accuracy of polarimetric information estimation.

2.3 CP Classification

For the classification, the Random Forest (RF) classifier (Breiman, 2001) based on the Scikit-learn module in Python

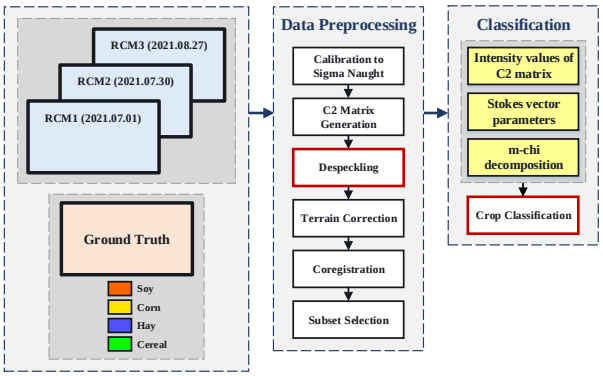

Figure 2. The workflow adopted in the paper.

(Pedregosa et al., 2011) is used in this paper. The RF hyperparameters, i.e., the number of trees in the forest, the maximum depth of the trees, the minimum number of samples required to split an internal node, and the maximum number of samples needed to be at a leaf node, were 50, 10, 10, and 3, respectively. It should be noted that the RF hyperparameters were fixed to the values mentioned to keep the classification circumstance identical for all CP input data despeckled based on various methods. Moreover, 70% of CP data was used for the training, while 30% was used for testing. Regarding reference data for the classification, the BDPPAD (Base de données des parcelles et productions agricoles déclarées) provided by La Financière agricole du Québec was utilized as the ground truth data. Figure 4, (a), (b), and (c) illustrate the RCM CP data after terrain correction, coregistration and subsetting. Furthermore, Figure 4 (d) demonstrates the ground truth and four main crop types in the study area, i.e., soy, corn, hay and cereal.

3. Experimental Results

3.1 Despeckling Performance Evaluation

Several no-reference indices were used to evaluate the despeckled data, such as Equivalent Number of Looks (ENL), Edge-Preservation Degree based on Ratio of Average (EPD-ROA), and Mean of Ratio image (MoR) (Farhadiani et al., 2019a). The ENL, computed in a homogeneous area from the SAR image, indicates the effectiveness of speckle suppression in homogeneous areas and can be computed as follows:

$$\text{ENL} = \frac{\mu}{\sigma} \tag{2}$$

where μ and σ are the mean and the standard deviation computed in a homogeneous area in the SAR image in intensity format. A better speckle reduction method should have higher ENL values. The EPD-ROA shows the capability to preserve edges and can be computed as (Feng et al., 2011):

$$\text{EPD-ROA} = \frac{\sum_{i=1}^{N} |I_{S1}(i)/I_{S2}(i)|}{\sum_{i=1}^{N} |I_{I1}(i)/I_{I2}(i)|} \tag{3}$$

where I_{S1} and I_{S2} demonstrate the adjacent pixel values of the despeckled image along the horizontal or vertical directions. Moreover, I_{I1} and I_{I2} illustrate the corresponding adjacent pixel values of image contaminated with speckle. Ideally,

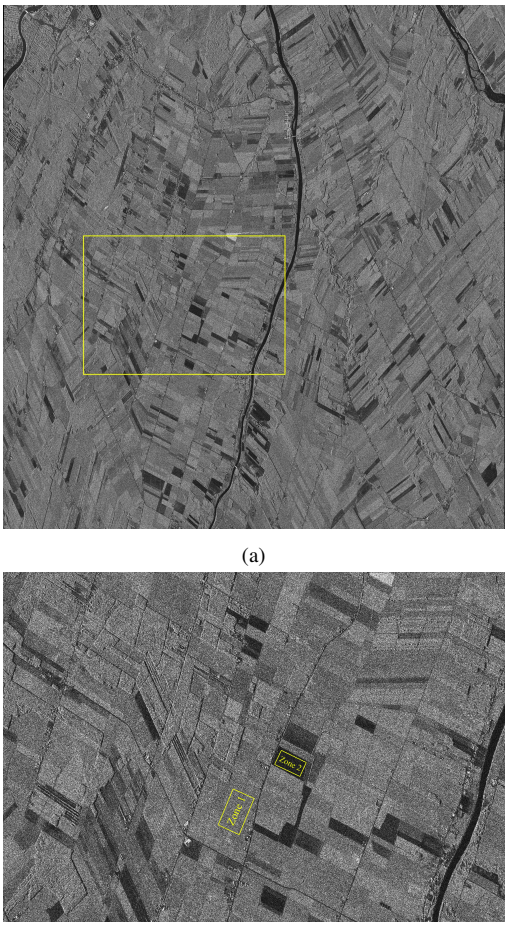

(a)

(b)

Figure 3. CP SAR image obtained on 27 August using RCM3 satellite. (a) the CP SAR image before terrain correction and coregistration, (b) the region of interest used for despeckling performance evaluation.

a higher EPD-ROA value indicates a better ability to preserve edges, with a value closer to one being optimal. The MoR between the SAR image prior to and following despeckling is also used as an indicator of the despeckling method's ability for radiometric preservation. In an ideal case, the MoR should be equal to one.

For each despeckling method, a range of parameters was selected for tuning, encompassing both small and relatively large values. This approach enables readers to discern the impact of each parameter on the degree of speckle suppression. Initially, the Number of Looks (L) was set to 1 for all methods where this parameter is adjustable. The sole parameter considered in the Box Car and Lee Refined filters is the window size, chosen as 5×5 (Box Car 5 and Lee Refined 5) or 11×11 (Box Car 11 and Lee Refined 11). Two adaptive neighborhood sizes were examined for the IDAN filter: 50 (IDAN 50) and 150 (IDAN 150). The tunable parameters of the Lee Sigma and Improved Lee Sigma are identical, with the Sigma parameter set to 0.9. Two combinations of target and filter window sizes were assessed: 3×3 and 9×9 (for Lee Sigma 39 and Improved Lee Sigma 39), and 5×5 and 11×11 (for Lee Sigma 511 and Improved Lee Sigma 511). Lastly, parameters such as window size, number of iterations, total weight for bias, and strong reduction were adjusted in the Lopez filter. The window sizes were 5×5 (Lopez 5) and 11×11 (Lopez 11), with a fixed

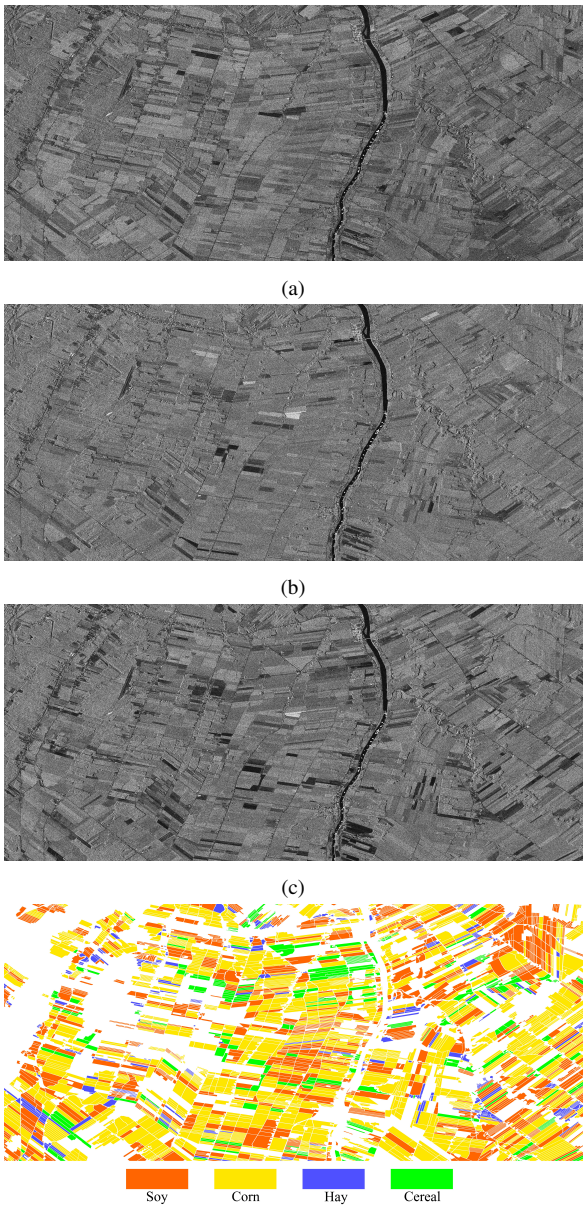

Figure 4. The processed CP SAR images for various dates, and the corresponding ground truth used for the classification. (a) 1 July 2021, (b) 30 July 2021, (c) 27 August 2021, (d) ground truth.

value of 1 for the number of iterations, the total weight for bias, and strong reduction.

Figure (5) illustrates despeckled CP SAR images using various despeckling techniques. Visually, it is apparent that increasing the window size enhanced speckle reduction across all adjustable despeckling methods. Specifically, the Box Car and Lopez filters significantly reduced speckle at the expense of over-smoothing the image. In contrast, the Lee Refined filter showed improved speckle suppression with larger window sizes but retained more edges. The Lee Sigma and Improved Lee Sigma filters balanced speckle reduction and detail preservation, displaying satisfactory results. However, the IDAN filter showed no notable visual improvement in speckle reduction when the Adaptive Neighborhood Size was increased from 50 to 150.

Table 2. Speckle Suppression Performance Evaluation based on Various Despeckled CP Data.

Methods	ENL		EPD-ROA ($\times 10^2$)		MoR
	Zone 1	Zone 2	Hor.	Vert.	
Box Car 5	9.06	9.24	13.93	9.00	0.96
Box Car 11	36.51	37.85	13.75	8.82	0.98
IDAN 50	5.46	5.64	16.11	10.51	1.43
IDAN 150	5.50	5.67	16.11	10.51	1.43
Lee Refined 5	6.87	6.99	14.32	9.34	1.23
Lee Refined 11	25.32	25.05	13.87	8.93	1.15
Lee Sigma 39	8.61	9.79	14.38	9.39	0.94
Lee Sigma 511	14.82	20.71	14.34	9.38	0.94
Im. Lee Sigma 39	10.87	12.07	14.12	9.16	0.98
Im. Lee Sigma 511	18.57	23.10	14.12	9.16	0.97
Lopez 5	9.06	9.24	13.93	9.01	0.96
Lopez 11	36.51	37.85	13.75	8.82	0.98

Table (2) provides numerical results computed using no-reference indices based on the C11 intensity image. According to the computed values for the ENL in two homogeneous zones shown in Figure 3, larger window sizes generally led to better speckle suppression, albeit EPD-ROA values confirmed that bigger window sizes resulted in edge smoothing. Notably, the Lee Sigma and Improved Lee Sigma filters were exceptions, effectively reducing speckle, particularly in homogeneous areas, while preserving edges. Interestingly, the Box Car and Lopez filters demonstrated similar results in speckle reduction. The least effective speckle reduction was observed with the IDAN filter, which was poor in terms of speckle suppression, edge preservation, and avoiding radiometric distortion. MoR values were acceptable in most methods and settings, indicating a proper ability of despeckling methods to avoid radiometric distortion. The Lee Refined filter, although effective in suppressing speckle and maintaining details, did not perform well in avoiding radiometric distortion.

3.2 Classification Performance Evaluation

Figure 6 displays classified CP SAR data processed with different speckle reduction techniques (the classified images based on despeckling using the IDAN and Lopez filters were not shown). Visual inspection revealed that smaller window sizes in the despeckling methods introduced a salt-and-pepper artifact in the classified images, which diminished as the window size increased. Mainly, classified CP data generated using larger parameters for each despeckling technique resulted in more homogeneous crop maps. This suggests that larger window settings effectively reduced noise while maintaining the integrity of the crop map imagery.

Table 3 presents the Overall Accuracy (OA), Kappa coefficient, and F1-score calculated for the classified CP data. As can be seen, larger window sizes used in despeckling consistently led to higher classification accuracies due to more effective speckle suppression. The Box Car 11 filter achieved the highest accuracy with an OA of 90.48%, a Kappa coefficient of 0.83, and an F1-score of 90.31%. Following closely, the Lopez 11 filter, which showed despeckling results similar to the Box Car filter, achieved the second-best accuracy. The classification accuracy based on the Improved Lee Sigma 511 were third highest, with an OA of 88.00%, Kappa of 0.79, and F1-score of 87.74%. The IDAN filter also observed the lowest classification accuracy, resulting in the least effective despeckling suppression. The results from the Lee Refined and Lee Sigma filters were better than those from the IDAN filter but lower than those from the Improved Lee Sigma.

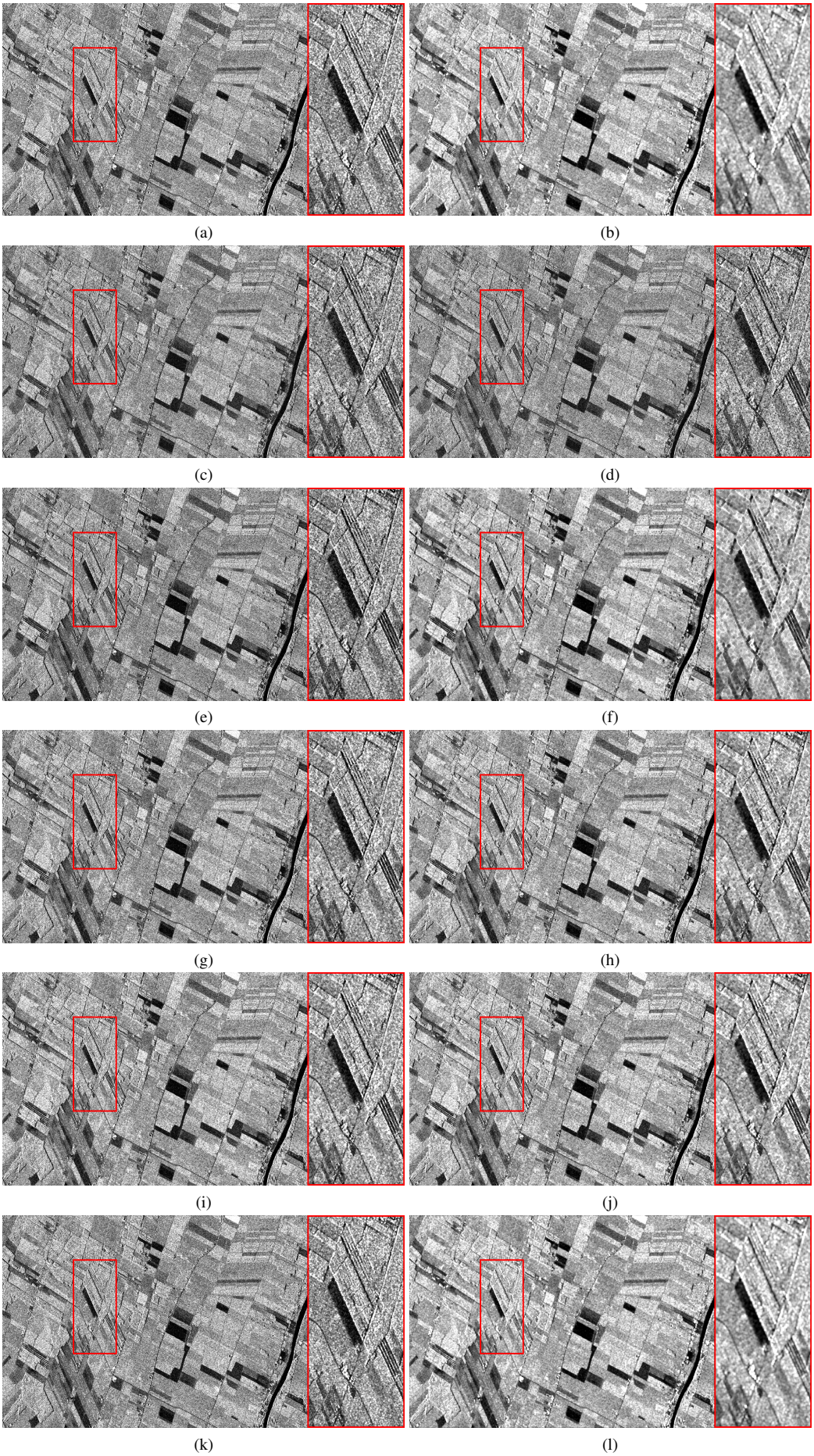

Figure 5. Despeckled CP SAR images based on various despeckling methods. (a) Box Car 5, (b) Box Car 11, (c) IDAN 50, (d) IDAN 150, (e) Lee Refined 5, (f) Lee Refined 11, (g) Lee Sigma 39, (h) Lee Sigma 511, (i) Improved Lee Sigma 39, (g) Improved Lee Sigma 511, (k) Lopez 5, (l) Lopez 11.

This contribution has been peer-reviewed.
https://doi.org/10.5194/isprs-archives-XLVIII-M-4-2024-17-2024

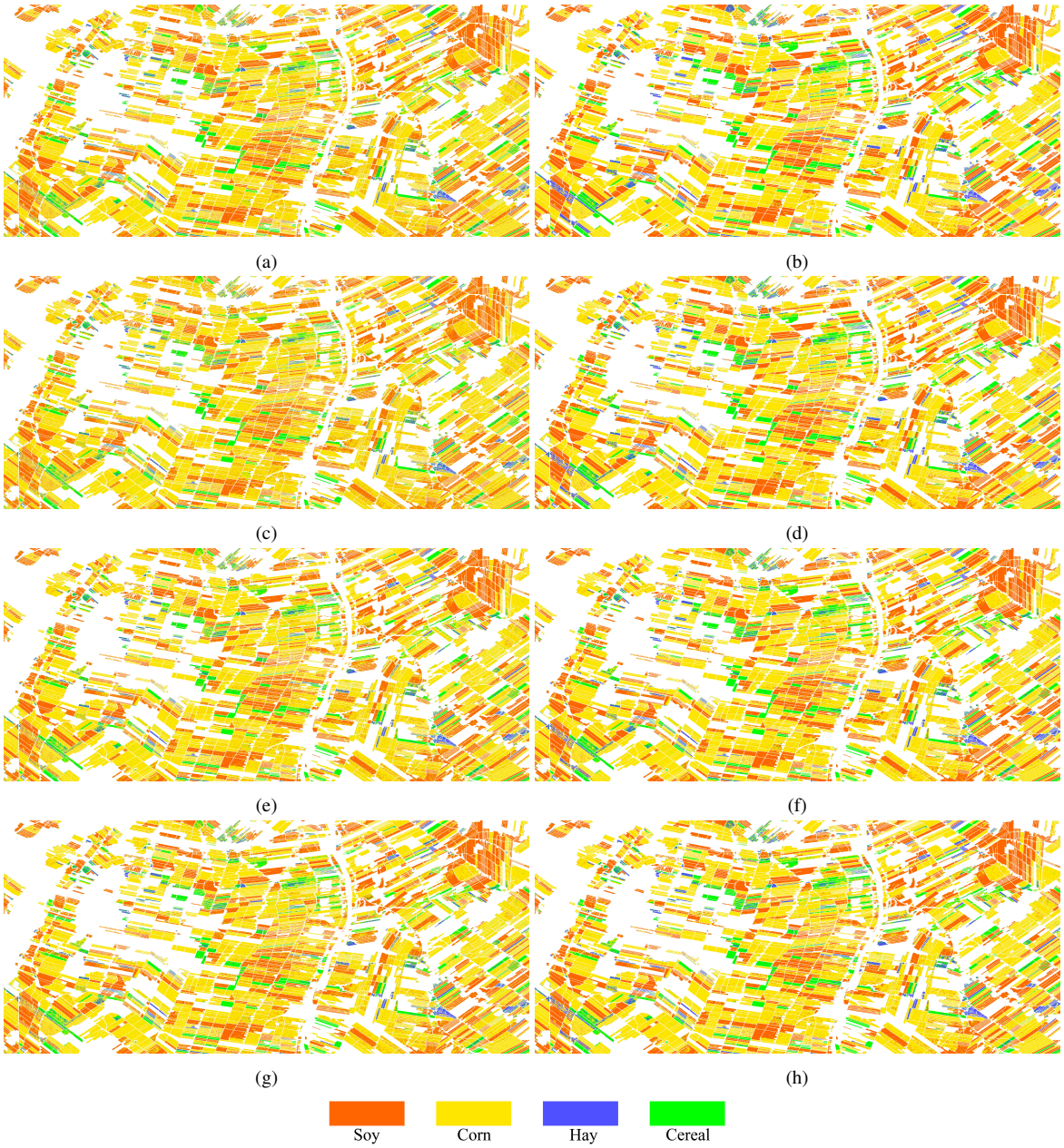

Figure 6. Final crop map derived from the RF classifier based on various despeckling methods. (a) Box Car 5, (b) Box Car 11, (c) Lee Refined 5, (d) Lee Refined 11, (e) Lee Sigma 39, (f) Lee Sigma 511, (g) Improved Lee Sigma 39, (h) Improved Lee Sigma 511.

It is important to note that larger window sizes do not invariably lead to better classification accuracy. Increasing the window size in filtering, while effective in speckle reduction, tended to over-smooth details, particularly edges. Since edges often define boundaries, i.e., transitions between agricultural land and natural or artificial structures, over-smoothing can blur these distinctions, potentially leading to inaccuracies and increased risk of misclassification. Hence, selecting the appropriate despeckling method requires careful consideration of the specific application demands to balance between speckle reduction and preserving edges in the SAR imagery. This balance is essential to ensure the highest possible accuracy in the crop classification results.

4. Conclusion

This study has provided some helpful insights into the effectiveness of various polarimetric despeckling filters and their impact on crop classification accuracy using the RCM CP SAR data. The study showed that while larger window sizes in despeckling filters generally enhanced speckle suppression, they may lead to edge over-smoothing, affecting the precise separation of different land features. The study also highlighted the superior performance of particular filters, like the Box Car, Lopez, and Improved Lee Sigma, contributing to higher crop classification accuracy. However, it also underscored the need to balance speckle suppression and detail preservation, as excessive smoothing can lead to misclassification risk in crop classification tasks.

Table 3. Classification Performance Evaluation based on Various Despeckled CP Data.

Methods	OA %	Kappa	F1-score %
Box Car 5	80.45	0.65	79.78
Box Car 11	90.48	0.83	90.31
IDAN 50	77.41	0.59	76.36
IDAN 150	77.58	0.59	76.55
Lee Refined 5	77.53	0.60	76.72
Lee Refined 11	87.41	0.78	87.19
Lee Sigma 39	82.51	0.69	81.90
Lee Sigma 511	87.47	0.78	87.17
Im. Lee Sigma 39	83.69	0.71	83.16
Im. Lee Sigma 511	88.00	0.79	87.74
Lopez 5	78.90	0.62	78.24
Lopez 11	88.50	0.80	88.29

References

Breiman, L., 2001. Random forests. *Machine learning*, 45, 5–32.

Collett, E., 2005. Field guide to polarization. Spie Bellingham, WA.

Dey, S., Bhattacharya, A., Ratha, D., Mandal, D., Frery, A. C., 2021. Target Characterization and Scattering Power Decomposition for Full and Compact Polarimetric SAR Data. *IEEE Transactions on Geoscience and Remote Sensing*, 59(5), 3981-3998.

Dingle Robertson, L., McNairn, H., Jiao, X., McNairn, C., Ihuoma, S. O., 2022. Monitoring crops using compact polarimetry and the RADARSAT constellation mission. *Canadian Journal of Remote Sensing*, 48(6), 793–813.

European Space Agency, 2024. Sentinel application platform (snap).

Farhadiani, R., Homayouni, S., Bhattacharya, A., Mahdianpari, M., 2022. SAR Despeckling Based on CNN and Bayesian Estimator in Complex Wavelet Domain. *IEEE Geoscience and Remote Sensing Letters*, 19, 1-5.

Farhadiani, R., Homayouni, S., Safari, A., 2019a. Hybrid SAR Speckle Reduction Using Complex Wavelet Shrinkage and Non-Local PCA-Based Filtering. *IEEE Journal of Selected Topics in Applied Earth Observations and Remote Sensing*, 12(5), 1489-1496.

Farhadiani, R., Homayouni, S., Safari, A., 2019b. IMPACT OF POLARIMETRIC SAR SPECKLE REDUCTION ON CLASSIFICATION OF AGRICULTURE LANDS. *The International Archives of the Photogrammetry, Remote Sensing and Spatial Information Sciences*, XLII-4/W18, 379–385. https://isprs-archives.copernicus.org/articles/XLII-4-W18/379/2019/.

Feng, H., Hou, B., Gong, M., 2011. SAR Image Despeckling Based on Local Homogeneous-Region Segmentation by Using Pixel-Relativity Measurement. *IEEE Transactions on Geoscience and Remote Sensing*, 49(7), 2724-2737.

Foucher, S., Landry, T., López-Martínez, C., Charbonneau, F., Gagnon, L., 2012. An evaluation of polsar speckle filters on compact-pol images. *2012 IEEE International Geoscience and Remote Sensing Symposium*, 5089–5092.

Lee, J.-S., 1981. Speckle analysis and smoothing of synthetic aperture radar images. *Computer Graphics and Image Processing*, 17(1), 24-32.

Lee, J.-S., 1983. A simple speckle smoothing algorithm for synthetic aperture radar images. *IEEE Transactions on Systems, Man, and Cybernetics*, SMC-13(1), 85-89.

Lee, J.-S., Grunes, M., de Grandi, G., 1999. Polarimetric SAR speckle filtering and its implication for classification. *IEEE Transactions on Geoscience and Remote Sensing*, 37(5), 2363-2373.

Lee, J.-S., Wen, J.-H., Ainsworth, T., Chen, K.-S., Chen, A., 2009. Improved Sigma Filter for Speckle Filtering of SAR Imagery. *IEEE Transactions on Geoscience and Remote Sensing*, 47(1), 202-213.

Lopez-Martinez, C., Fabregas, X., 2008. Model-Based Polarimetric SAR Speckle Filter. *IEEE Transactions on Geoscience and Remote Sensing*, 46(11), 3894-3907.

Luo, J., Zhang, L., Dong, J., Lopez-Sanchez, J. M., Wang, Y., Feng, H., Liao, M., 2023. Despeckling Multitemporal Polarimetric SAR Data Based on Tensor Decomposition. *IEEE Journal of Selected Topics in Applied Earth Observations and Remote Sensing*, 16, 9858-9873.

Mullissa, A. G., Persello, C., Reiche, J., 2022. Despeckling Polarimetric SAR Data Using a Multistream Complex-Valued Fully Convolutional Network. *IEEE Geoscience and Remote Sensing Letters*, 19, 1-5.

Pedregosa, F., Varoquaux, G., Gramfort, A., Michel, V., Thirion, B., Grisel, O., Blondel, M., Prettenhofer, P., Weiss, R., Dubourg, V., Vanderplas, J., Passos, A., Cournapeau, D., Brucher, M., Perrot, M., Édouard Duchesnay, 2011. Scikit-learn: Machine Learning in Python. *Journal of Machine Learning Research*, 12(85), 2825-2830. http://jmlr.org/papers/v12/pedregosa11a.html.

Pottier, E., Ferro-Famil, L., Fitrzyk, M., Desnos, Y.-L., 2018. Polsarpro-bio: An esa educational toolbox used for self-education in the field of polsar, pol-insar and pol-tomosar data analysis. *IGARSS 2018 - 2018 IEEE International Geoscience and Remote Sensing Symposium*, 6568–6571.

Raney, R. K., Brisco, B., Dabboor, M., Mahdianpari, M., 2021. RADARSAT Constellation Mission's operational polarimetric modes: A user-driven radar architecture. *Canadian Journal of Remote Sensing*, 47(1), 1–16.

Raney, R. K., Cahill, J. T., Patterson, G. W., Bussey, D. B. J., 2012. The m-chi decomposition of hybrid dual-polarimetric radar data. *2012 IEEE International Geoscience and Remote Sensing Symposium*, 5093–5096.

Vasile, G., Trouve, E., Lee, J.-S., Buzuloiu, V., 2006. Intensity-driven adaptive-neighborhood technique for polarimetric and interferometric SAR parameters estimation. *IEEE Transactions on Geoscience and Remote Sensing*, 44(6), 1609-1621.

Wang, C., Guo, B., 2023. A Double Residual Iterative Regularization Method for SAR Image Despeckling. *IEEE Geoscience and Remote Sensing Letters*, 20, 1-5.